MODELING OF LARGE DEFORMATIONS OF SATURATED SOILS DURING FAULT SURFACE RUPTURES

Jörgen JOHANSSON[1] and Kazuo KONAGAI[2]

Abstract: A two phase formulation is implemented into the material point method with the purpose of modeling large deformations of saturated soils during surface fault ruptures. Numerical simulations of fault surface rupture model experiments show the abilities of the developed numerical tool. Problems related to incompressibility constraints are discussed and circumvented for pure seepage problems whereas for solid-fluid deformations there is a need for further improvement of the tool.

Key Words: Large deformation, saturated soil, fault surface rupture experiment, incompressibility.

INTRODUCTION

The 1999 earthquakes in Taiwan and Turkey has shown how great a risk fault surface ruptures are to human lives, buildings and infrastructure. Even though fault surface rupturing is not a new problem, there are very few building codes in the world containing any type provisions for reducing the risks. This may be due to the infrequent occurrence of fault surface ruptures, the great difficulty in preventing damage to infrastructure and buildings affected by the ruptures and also the difficult task of estimating possible deformations due to many unknown factors such as possible location; geometry and motion of the fault; and mechanical properties of the soil deposit.

In California, United States; New Zealand; and also in Taiwan, after the 1999 earthquake, so called fault zoning acts have been established. A fault zoning act prevents construction within a certain distance of the known fault line and may be one way of reducing the risks for new buildings and infrastructure, but for structure already built along a fault line other remedial measures are needed, further more the fault zoning act does not say anything about the possible extent of deformations and/or what are the probability of occurrence of these deformations.

In highly populated countries such as Japan and other east and south-east Asian countries it is difficult to impose a fault-zoning act due to the lack of space. In these countries building code provisions based on engineering principles are needed as to allow for construction along fault-lines if certain design requirements are met. Such building code provisions would also be attractive for less populated countries, such as United States and New Zealand, as well, since it may allow for more economical construction.

Another issue is the difference between strike-slip and dip-slip faults. The deformations along a strike-slip seem to be concentrated in a narrower zone along the fault line whereas the deformations along a dip-slip fault may affect areas further away from the fault line (Mukoyama, 2000). In Japan there are some 90 dip-slip fault systems with several faults in each system and with a lot of buildings and infrastructure along them.

[1]Research Associate, Earthquake Engineering Laboratory
[2]Professor, Ditto

To provide results in the form of possible extent and probabilities of deformation along these fault lines, much research is needed. Specifically numerical tools are needed to estimate possible deformations induced in structures in and on top of soil deposit affected by fault surface rupture. Within here is described a numerical tool that allow for the numerical simulations of large deformations related to fault surface ruptures. Numerical results are compared with results of some recently performed experiments.

NUMERICAL TOOL

The developed numerical tool is based on the Material Point Method first described in (Sulsky et al., 1994). It is a fairly new method for solving problems in solid mechanics (Sulsky et al., 1995) and is an extension of a hydrodynamics code called FLIP (Burgess et al., 1992) which, in turn, evolved from the Particle-in-Cell Method for fluid flow(Harlow, 1964).

Solid-fluid interaction formulation

A coupled solid fluid (u-w) scheme described by (Chan et al., 1991) is adopted and adjusted for implementation in the Material Point Method. It is assumed that the soil deposit is fully saturated, Darcy's law is valid, solid grains are incompressible, and thermal changes are negligible. Further assumptions are given below along with the derivation. The governing equations are given for a Lagrangian frame moving with the solid-fluid mixture in terms of solid-fluid mixture momentum equilibrium (see e.g. Zienkiewicz et al. (1990); Lewis and Schrefler (1998) or chapter 2 in Zienkiewicz et al. (1999)) ,

$$\sigma_{ij,j} - \rho_m \ddot{u}_i - \rho_f \left(\ddot{w}_i + \underline{\dot{w}_j \dot{w}_{i,j}} \right) + \rho_m b_i = 0, \tag{1}$$

fluid equilibrium,

$$-p_{,i} - [k_{ki}]^{-1} \dot{w}_k - \rho_f \ddot{u}_i - \frac{\rho_f}{n} \left(\ddot{w}_i + \underline{\dot{w}_j \dot{w}_{i,j}} \right) + \rho_f b_i = 0, \tag{2}$$

and mass conservation,

$$\dot{w}_{i,i} + \dot{\varepsilon}_{ii} + \frac{n\dot{p}}{K_f} = 0. \tag{3}$$

For a description and sign convention of the variables in above formulas are see Table 1 . Equation (2) is further simplified by assuming isotropic permeability $k_{ki} = k$ and neglecting the underlined convective terms to obtain the two governing equations

$$\sigma_{ij,j} - \rho_m \ddot{u}_i - \rho_f \ddot{w}_i + \rho_m b_i = 0, \tag{4}$$

$$-p_{,i} - \frac{\dot{w}_i}{k} - \rho_f \ddot{u}_i - \frac{\rho_f}{n} \ddot{w}_i + \rho_f b_i = 0 \tag{5}$$

where the total stresses, σ_{ij}, are obtained from the effective stresses and pore water pressure

$$\sigma_{ij} = \sigma'_{ij} - \delta_{ij} p \tag{6}$$

and the effective stresses

$$\dot{\sigma}'_{ij} = f\left(\sigma'_{ij}, \dot{\varepsilon}_{ij}, \ldots\right) \tag{7}$$

are explicitly obtained from an appropriate constitutive law e.g. hypo-plasticity (Kolymbas, 19), which is used in the numerical examples below. For the explicit scheme derived below Equation (3) is used for updating the excessive pore pressure by multiplying with the time increment, Δt, to obtain

$$\Delta p = \Delta t \dot{p} = -\Delta t \frac{K_f}{n} \left(\dot{w}_{i,i} + \dot{\varepsilon}_{ii} \right). \tag{8}$$

On the other hand if an implicit scheme is desired, Equation (3) should be integrated in time to obtain a direct expression for the pore water pressure and inserted in to Equation (5) and it may be easier to use the absolute displacement of water instead of the relative displacements as here (see further chapter 3 in Zienkiewicz et al. (1999)).

Table 1: Variable description.

Variable	Description	Remark
σ_{ij}	Total Stress	Compression negative
u_i	Solid matrix displacements	
$\rho_m = (1-n)\rho_s + n\rho_f$	Solid-Fluid Mixture density	
ρ_f	Fluid density	
ρ_s	Solid density	
n	Porosity	
w_i	Water displacement relative to solid matrix	
b_i	Body force on solid-fluid mixture	e.g. gravity
p	Pore pressure	Compression positive
$k_{ki} = \frac{k'_{ki}}{\rho_f g}$	Permeability	Unit: $[L^3T^{-1}M^{-1}]$
k'_{ki}	Hydraulic Conductivity	Unit: $[LT^{-1}]$
g	gravity	
ε_{ii}	Volumetric strain of solid-fluid mixture	
K_f	Fluid bulk modulus	

Finite element discretization

The governing equations and boundary conditions are first for clarity discretized spatially with finite elements to establish the equation system and then the material point concept is introduce in the following section. The mixture and fluid displacements take the following forms:

$$u_i(x_i,t) = u_I(t)N_I^u(x_i), \quad w_i(x_i,t) = w_I(t)N_I^w(x_i), \quad I = 1,...,N_n \tag{9}$$

Where the $N's$ are finite element shape functions. Upper case letters represent nodal numbers, lower case letters are refers to Cartesian coordinate and summation convention is applied. Lower case letters m, c, and f are applied to mixture, coupling and fluid terms. (The notation is somewhat relaxed to reduce space and time of the derivation, hopefully the concept and procedures will be clear to the any reader anyway). Multiplying Equation (4) and Equation (5) by the interpolation function N_i^u and N_i^w, respectively as weighting functions and integrate over the domain the following two equations are obtained.

$$\int_\Omega N_I^u(\sigma_{ij,j} - \rho_m\ddot{u}_i - \rho_f\ddot{w}_i + \rho_m b_i)\,d\Omega = 0, \tag{10}$$

$$\int_\Omega N_I^w\left(-p_{,i} - \frac{\dot{w}_i}{k} - \rho_f\ddot{u}_i - \frac{\rho_f}{n}\ddot{w}_i + \rho_f b_i\right)d\Omega = 0 \tag{11}$$

Integrating first term of the Equation (10) by parts gives

$$\int_\Omega N_I^u\sigma_{ij,j}d\Omega = \int_S N_I^u n_i\sigma_{ij}dS - \int_\Omega N_{I,j}^u\sigma_{ij}d\Omega = f_{mIi}^{ext,tractions} - f_{mIi}^{int} \tag{12}$$

where $f_{mIi}^{ext,tractions}$ and $f_{mIi}^{int}$are external traction forces and internal forces respectively. The second term in Equation (10) gives the mixture mass matrix

$$-\int_\Omega N_I^u\rho_m\ddot{u}_i d\Omega = -\int_\Omega N_I^u\rho_m N_J^u d\Omega\ddot{u}_{Ji} = -M_{mIJ}\ddot{u}_{Ji}, \tag{13}$$

the third term becomes the mixture-fluid coupling mass matrix

$$-\int_\Omega N_I^u\rho_f\ddot{w}_i d\Omega = -\int_\Omega N_I^u\rho_f N_J^w d\Omega\ddot{w}_{Ji} = -M_{cIJ}\ddot{w}_{Ji} \tag{14}$$

and the final term gives the body-forces applied to the solid-fluid mixture

$$\int_{\Omega} N_I^u \rho_m b_i d\Omega = f_{mIi}^{bodyforces}. \tag{15}$$

Now turning to the second governing Equation (11) the first term becomes

$$-\int_{\Omega} N_I^w p_{,i} d\Omega = -\int_S N_I^w n_i p dS + \int_{\Omega} N_{I,i}^w p d\Omega = f_{fIi}^{ext,pressure} + f_{fIi}^{int} \tag{16}$$

which is the externally applied pressure on the fluid and internal forces due to the pore pressure. The second term becomes

$$-\int_{\Omega} N_I^w \frac{\dot{w}_i}{k} d\Omega = -\int_{\Omega} N_I^w \frac{1}{k} N_J^w d\Omega \dot{w}_{Ji} = -C_{fIJ} \dot{w}_{Ji} \tag{17}$$

where C_{fIJ} is the fluid damping matrix. The third term becomes

$$-\int_{\Omega} N_I^w \rho_f \ddot{u}_i d\Omega = -\int_{\Omega} N_I^w \rho_f N_J^u d\Omega \ddot{u}_{Ji} = -M_{cJI} \ddot{u}_{Ji} \tag{18}$$

where $M_{cJI} = M_{cIJ}^T$ is the fluid-mixture coupling mass matrix which is transpose of the mixture-fluid coupling mass matrix. From the fourth term the fluid mass matrix is given as

$$-\int_{\Omega} N_I^w \frac{\rho_f}{n} \ddot{w}_i d\Omega = -\int_{\Omega} N_I^w \frac{\rho_f}{n} N_J^w d\Omega \ddot{w}_{Ji} = -M_{fIJ} \ddot{w}_{Ji} \tag{19}$$

and finally the last term gives the body forces applied on the fluid

$$\int_{\Omega} N_I^w \rho_f b_i d\Omega = f_{fIi}^{bodyforces}. \tag{20}$$

The above terms from Equations (10)and (11) is assembled into the equation system

$$\begin{bmatrix} M_{mIJ} & M_{cIJ} \\ M_{cIJ}^T & M_{fIJ} \end{bmatrix} \begin{Bmatrix} \ddot{u}_{Ji} \\ \ddot{w}_{Ji} \end{Bmatrix} + \begin{bmatrix} C_m & \mathbf{0} \\ \mathbf{0} & C_{fIJ} \end{bmatrix} \begin{Bmatrix} \dot{u}_{Ji} \\ \dot{w}_{Ji} \end{Bmatrix} + \begin{bmatrix} f_{mIi}^{int} & \mathbf{0} \\ \mathbf{0} & -f_{fIi}^{int} \end{bmatrix} = \begin{Bmatrix} f_{mIi}^{ext,tractions} + f_{mIi}^{bodyforces} \\ f_{fIi}^{ext,pressure} + f_{fIi}^{bodyforces} \end{Bmatrix} \tag{21}$$

where C_m is an artificial damping matrix applied to the solid-fluid mixture.

Material point discretization and a simple modification

Here follows the derivation of the material point version of (21). In the original material point method a material density is represented discretely by material points with a constant mass according to a Dirac delta function as

$$\rho(x_i,t) = \sum_{p=1}^{N_p} m_p \delta(x_i - X_p(t)) \tag{22}$$

since the material points are following the Lagrangian frame. If we use a Lagrangian frame for representing the solid part of the porous material its density can be written as:

$$\rho_s(x_i,t) = \sum_{p=1}^{N_p} m_{sp} \delta(x_i - X_p(t)). \tag{23}$$

The pore fluid (water) percolates with the velocity w_i relative to the solid's Lagrangian frame. One way to deal with this would be to introduce completely Lagrangian fluid material points. But this would

require more exchange of information since e.g. the fluid pressure at the fluid points would have to be interpolated to the solid points to compute the effective stresses which is used in relevant constitutive laws. Under the assumption that the fluid percolation velocity relative to the solid is small we can keep the location fluid points and solid points in the same Lagrangian point through-out the calculation there is no need for the extra information exchange and thus a relative decrease in computation time and less tedious coding are realized. To allow for this simplification we need to account for the fluid percolation relative to the solid by correspondingly changing the fluid point masses according to the divergence of the relative velocity

$$\Delta m_{fp} = -\Delta t \rho_f V_{mp} \dot{w}_{i,i} \tag{24}$$

where the fluid density ρ_f is assumed to be constant even though the water is slightly compressible. The total mass of a solid-fluid mixture material point is now represented by a sum of the constant solid mass and the variable fluid mass

$$m_{mp} = m_{sp} + m_{fp} \tag{25}$$

and the solid-fluid mixture density is

$$\rho_m(x_i,t) = \sum_{p=1}^{N_p} (m_{sp} + m_{fp}) \delta(x_i - X_p(t)). \tag{26}$$

The volume of a material point representing the solid-fluid mixture becomes

$$V_{mp} = \frac{m_{sp} + m_{fp}}{\rho_m} \tag{27}$$

which has to be updated according to the volumetric change of the mixture, $\dot{\varepsilon}_{ii}$.

Applying the concept of discrete density to the individual terms in (21) and invoking

$$\int_\Omega d\Omega = \sum_{p=1}^{N_p} V_{mp} \tag{28}$$

where N_p is the number of material points within Ω, we derive the material point formulation as follows. The solid-fluid mixture mass matrix becomes

$$M_{mIJ} = \int_\Omega N_I^u \rho_m N_J^u d\Omega = \sum_{p=1}^{N_p} N_I^u (m_{sp} + m_{fp}) N_J^u, \tag{29}$$

the coupling solid-fluid mass matrices, with $\rho_f V_{mp} = m_{fp}/n$ become

$$M_{cIJ} = \int_\Omega N_I^u \rho_f N_J^w d\Omega = \sum_{p=1}^{N_p} N_I^u \rho_f V_{mp} N_J^w = \sum_{p=1}^{N_p} N_I^u \frac{m_{fp}}{n} N_J^w = M_{cJI}^T \tag{30}$$

and the fluid mass matrix becomes

$$M_{fIJ} = \int_\Omega N_I^w \frac{\rho_f}{n} N_J^w d\Omega = \sum_{p=1}^{N_p} N_I^u \frac{\rho_f}{n} V_{mp} N_J^w = \sum_{p=1}^{N_p} N_I^u \frac{m_{fp}}{n^2} N_J^w. \tag{31}$$

The solid-fluid mixture artificial damping matrix, C_m, remains the same as in the FE discretization, but the fluid damping matrix, C_{fIJ}, changes to

$$C_{fIJ} = \int_\Omega N_I^w \frac{1}{k} N_J^w d\Omega = \sum_{p=1}^{N_p} N_I^w \frac{1}{k} V_{mp} N_J^w = \sum_{p=1}^{N_p} N_I^w \frac{\rho_f g}{k'} V_{mp} N_J^w = \sum_{p=1}^{N_p} N_I^w \frac{g}{k'} \frac{m_{fp}}{n} N_J^w. \tag{32}$$

The internal forces of the solid-fluid mixture and the fluid now become, respectively

$$f_{mIi}^{int} = \int_{\Omega} N_{I,j}^{u} \sigma_{ij} d\Omega = \sum_{p=1}^{N_p} N_{I,j}^{u} V_{mp} \sigma_{ij} \tag{33}$$

and

$$f_{fIi}^{int} = \int_{\Omega} N_{I,i}^{w} p d\Omega = \sum_{p=1}^{N_p} N_{I,i}^{w} V_{mp} p. \tag{34}$$

Here the volume of the solid-fluid mixture material point is invoked again since the governing Equation (5) is derived with respect to the total volume of the solid-fluid mixture. Then all terms on the left hand side in Equation system (21) have been changed to material point equivalent terms. On the right hand side the solid-fluid mixture external traction, $f_{mIi}^{ext,tractions}$, and the fluid external pressure, $f_{fIi}^{ext,pressure}$, remains the same as in the FE discretization. The body force terms of the solid-fluid mixture and the fluid becomes, respectively

$$f_{mIi}^{bodyforces} = \int_{\Omega} N_I^u \rho_m b_i d\Omega = \sum_{p=1}^{N_p} N_I^u \left(m_{sp} + m_{fp}\right) b_{pi} \tag{35}$$

$$f_{fIi}^{bodyforces} = \int_{\Omega} N_I^w \rho_f b_i d\Omega = \sum_{p=1}^{N_p} N_I^w \frac{m_{fp}}{n} b_{pi} \tag{36}$$

where b_{pi} is the body force acting on the solid-fluid mixture material point.

Time discretization

To keep the current simple explicit scheme it is desirable to solve the Equations system (21) by diagonalizing/lumping the mass and damping matrices and using staggered central differences. The lumping results in block diagonal system

$$\begin{bmatrix} M_{mI} & M_{cI} \\ M_{cI} & M_{fI} \end{bmatrix}^k \begin{Bmatrix} \dot{u}_{Ii}^k \\ \dot{w}_{Ii}^k \end{Bmatrix} + \begin{bmatrix} C_{mI} & \mathbf{0} \\ \mathbf{0} & C_{fI} \end{bmatrix}^k \begin{Bmatrix} \dot{u}_{Ii}^k \\ \dot{w}_{Ii}^k \end{Bmatrix} + \begin{bmatrix} f_{mIi}^{int} & \mathbf{0} \\ \mathbf{0} & -f_{fIi}^{int} \end{bmatrix}^k =$$

$$= \begin{Bmatrix} f_{mIi}^{ext,tractions} + f_{mIi}^{bodyforces} \\ f_{fIi}^{ext,pressure} + f_{fIi}^{bodyforces} \end{Bmatrix}^k \tag{37}$$

where the diagonal consists of 2 by 2 matrices which has to be solved for each degree of freedom at discrete times, t^k. I is the node number, i is the Cartesian direction and the k on the matrices means that they are computed for each time step. Approximating the mixture accelerations and velocities with

$$\dot{u}_{Ii}^k = \frac{1}{\Delta t}\left(\dot{u}_{Ii}^{k+1/2} - \dot{u}_{Ii}^{k-1/2}\right) \tag{38}$$

respectively

$$u_{Ii}^k = \frac{1}{2}\left(\dot{u}_{Ii}^{k+1/2} + \dot{u}_{Ii}^{k-1/2}\right), \tag{39}$$

and likewise the fluid accelerations and velocities, the lumped system (37) is rewritten for each degree of freedom

$$\frac{1}{\Delta t}\tilde{M}_I \dot{\tilde{u}}_{Ii}^{k+1/2} + \frac{1}{2}\tilde{C}_I \dot{\tilde{u}}_{Ii}^{k+1/2} = \tilde{F}_{Ii}^k + \frac{1}{\Delta t}\tilde{M}_I \dot{\tilde{u}}_{Ii}^{k-1/2} - \frac{1}{2}\tilde{C}_I \dot{\tilde{u}}_{Ii}^{k-1/2} \tag{40}$$

where the $\tilde{M}_I$ and $\tilde{C}_I$ represents the terms collected from the corresponding matrices, $\tilde{F}_{Ii}$ contains the collected internal, external and body-forces, $\dot{\tilde{u}}_{Ii}$ is the velocities vector

$$\dot{\tilde{u}}_{Ii} = \begin{Bmatrix} \dot{u}_{Ii} \\ \dot{w}_{Ii} \end{Bmatrix} \tag{41}$$

and Δt is the time step. Multiplying Equation (40) with the time step and collecting the terms on the left hand side we obtain

$$\left(\tilde{M}_I + \frac{\Delta t}{2}\tilde{C}_I\right)\dot{\tilde{u}}_{Ii}^{k+1/2} = \Delta t\tilde{F}_{Ii}^{k} + \tilde{M}_I\dot{\tilde{u}}_{Ii}^{k-1/2} - \frac{\Delta t}{2}\tilde{C}_I\dot{\tilde{u}}_{Ii}^{k-1/2} \tag{42}$$

from which $\dot{\tilde{u}}_{Ii}$ can be solved for

$$\dot{\tilde{u}}_{Ii}^{k+1/2} = \left(\tilde{M}_I + \frac{\Delta t}{2}\tilde{C}_I\right)^{-1}\left(\Delta t\tilde{F}_{Ii}^{k} + \tilde{M}_I\dot{\tilde{u}}_{Ii}^{k-1/2} - \frac{\Delta t}{2}\tilde{C}_I\dot{\tilde{u}}_{Ii}^{k-1/2}\right). \tag{43}$$

The new velocities are used to update the position of the solid-fluid mixture material points, computation of the strain rates for the stress updates, and fluid divergence for updating the mass of the fluid material points. See the appendix for a derivation of explicit formulas for the solid and fluid velocities.

Initial conditions

To start the time stepping procedures it is assumed that the initial mixture and fluid velocities are zero,

$$\dot{\tilde{u}}_{Ii}^{k=0} = 0, \tag{44}$$

which implies

$$\dot{\tilde{u}}_{Ii}^{1/2} = -\dot{\tilde{u}}_{Ii}^{-1/2}. \tag{45}$$

Putting Equation (45) into Equation (42) gives the velocities

$$\dot{\tilde{u}}_{Ii}^{k=1/2} = \frac{\Delta t}{2}\tilde{M}_I^{-1}\tilde{F}_{Ii}^{k=0} \tag{46}$$

and the velocity increments

$$\Delta\dot{\tilde{u}}_{Ii}^{k=1/2} = \frac{\Delta t}{2}\tilde{M}_I^{-1}\tilde{F}_{Ii}^{k=0}. \tag{47}$$

The inverse to the mass matrix is

$$\tilde{M}_I^{-1} = \begin{bmatrix} M_{ml} & M_{cl} \\ M_{cl} & M_{fl} \end{bmatrix}^{-1} = \frac{1}{M_{ml}M_{fl} - M_{cl}^2}\begin{bmatrix} M_{fl} & -M_{cl} \\ -M_{cl} & M_{ml} \end{bmatrix} \tag{48}$$

$$\begin{aligned} \dot{u}_{Ii}^{1/2} = & \frac{\Delta t/2}{M_{ml}M_{fl} - M_{cl}^2}\left[M_{fl}\left(f_{mli}^{ext,tractions} + f_{mli}^{bodyforces} - f_{mli}^{int}\right) - \right. \\ & \left. M_{cl}\left(f_{fli}^{ext,pressure} + f_{fli}^{bodyforces} + f_{fli}^{int}\right)\right] \end{aligned} \tag{49}$$

$$\begin{aligned} \dot{w}_{Ii}^{1/2} = & \frac{\Delta t/2}{M_{ml}M_{fl} - M_{cl}^2}\left[-M_{cl}\left(f_{mli}^{ext,tractions} + f_{mli}^{bodyforces} - f_{mli}^{int}\right) + \right. \\ & \left. M_{ml}\left(f_{fli}^{ext,pressure} + f_{fli}^{bodyforces} + f_{fli}^{int}\right)\right]. \end{aligned} \tag{50}$$

Boundary conditions

For the analysis of the numerical examples given below three different combinations of boundary conditions have been used:

1. Both solid and fluid velocities are prescribed.
2. Solid velocities are prescribed and fluid velocities are unprescribed.

3. Both solid and fluid velocities are non-prescribed.

Combination 1 is used for the motion perpendicular to an impermeable boundary. The second combination is used for the motion parallel to a rough boundary were solid velocities are prescribed and the fluid is free to move parallel along the wall or for motion perpendicular to a permeable wall. The third type is used for the motion parallel to a slippery boundary. In the explicit scheme adopted here type 1 is implemented by computing the appropriate velocity increments and for type 3 nothing is done since it really no constraints are applied to the velocities. Type 2 requires one to solve for forces acting on the solid corresponding to the prescribed velocities from Equation (A4) and use these forces to compute the fluid velocity increments with Equation (A7). Other possible boundary conditions would include external nodal forces due to pressure on the fluid, point or linear loads on the solid-fluid mixture.

Critical time-step and stability

A discussion on the critical time step for 1-D explicit MPM is available in Wieckowski et al. (1999). In general a smaller time-step then for a regular explicit FEM is required.

The stability of the Material Point Method is highly dependent on the order of updating stress strain. The original procedure was modified by Sulsky et al. (1995) and a higher stability was achieved. Bardenhagen (2002) suggested a different update which also improves stability. The main difference between the two modifications is a slight difference in conservation of energy.

SEEPAGE PROBLEM

A simple 2-D plane strain seepage problem has been chosen to show the abilities and problems with the method. It is shown that the specific way of computing strains and internal forces are very important to obtain a reliable results. An elastic soil in gravitational equilibrium is contained in a box 2.5 by 1 meter and is surrounded by impermeable vertical walls with a bottom that can allow fluid flow out of the box at the left most 0.75 meters. The input data shown in Table2 are all the same for the 4 cases and the initial

Table 2: Input data for seepage problem.

Parameter	Value
Solid Elastic Modulus	$1.0 \cdot 10^6$ Pa
Poisson ratio, v	0.3
Fluid Bulk Modulus	$1.0 \cdot 10^8$ Pa
Fluid density	1000 kg/m^3
Solid density	2650 kg/m^3
Porosity	0.5
Hydraulic Conductivity	$1.0 \cdot 10^{-2}$ m/s
gravity	9.82 N/kg

pressure are shown in 1 . The problem is solved with different ways of strain computations with and without averaging the fluid pressure and its increment. The solid velocities are damped out with high viscous mass proportional damping as to avoid any oscillations of the solid which would affect the fluid flow. Cases with different amount of damping were computed to confirm that the neither directions nor the magnitudes of the fluid velocities were affected by the damping value. Figure 2 shows fluid velocities and pressures results from 4 different cases which are described below (see also Table 3).

Case 1: The strains are computed with usual derivative of the bilinear interpolation. As seen in Figure 2 (a) and (b) the fluid pressure is unstable and show a typical checker boarding due to the so called Babuska-Brezzi instability (see further(Hughes, 1983) or (Bathe, 1996)).

Case2: To circumvent the Babuska-Brezzi instability the B-bar method (Hughes, 1983) of computing strains and internal forces where adopted. As a special case of the B-bar method the mean dilatation method (Nagtegaal et al., 1974) is used here. The result was improved slightly but still a the checker boarding is observed.

Case 3: Hughes (Hughes, 1983) also discusses the need for smoothing the pressure and its increments. The strains and internal forces are compute as for Case 1 but the pressure and its increment is averaged for each element. Now the fluid velocity show a more physical pattern and the pressure distribution is smooth and goes toward zero along the left boundary which is natural for a material in free flow. One can imagine a small stone falling through air (neglecting the air resistance) it will be completely stress free.

Case 4: In this case the B-bar method from case 2 was combined with an averaging of the fluid pressure and as seen the result is equal to the ones of case 3 showing the importance of smoothing the pressures.

FAULT SURFACE RUPTURE EXPERIMENTS

To obtain experimental results in order to verify the numerical model and to study in detail the effects on the deformation buildup due to a dip-slip fault when pore water is present in a soil a new model experiment has been designed.

Experiment setup and preparation

A box measuring 1.2 by 1.2 meters in plan and 60 cm deep was constructed (see Figure 3) . A 40 cm diameter piston in the middle of the box, which is attached to a hydraulic actuator, is used to lift/push up the soil to create the fault surface rupture. Toyoura sand with a mean diameter, D_{50}, of 0.2 mm was pluviated into the box to assure repeatability and homogeneity. To be able to see the induced deformation the sand deposit was inter-layered with thin (3-5 mm) horizontal layers of colored toyoura sand every 5 cm (see Figure 4). The sand density was 1580 kg/m^3corresponding to a void ratio, e, of 0.68.

Experiment results

After the experiment the dry sand was first saturated and immediately drained and the saturated sand was drained . The moist sand could then be easily cut along a vertical planes as to study the built up deformations. Two cuts from a dry and a saturated case are shown in Figure 4. The soil deformation has localized into narrow shear-band and offset the dark horizontal lines. The shear-band or rupture planes are also readily seen as brighter lines crossing through darker less deformed zones.

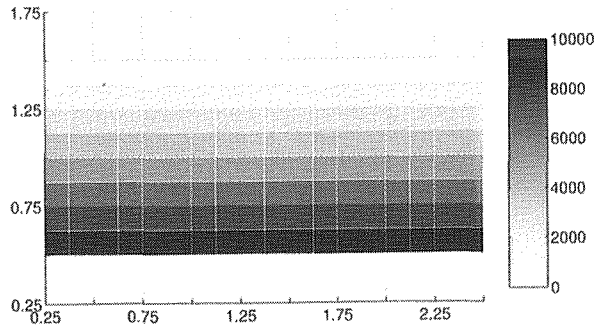

Figure 1: Initial pressure [Pa] due to gravity in seepage example

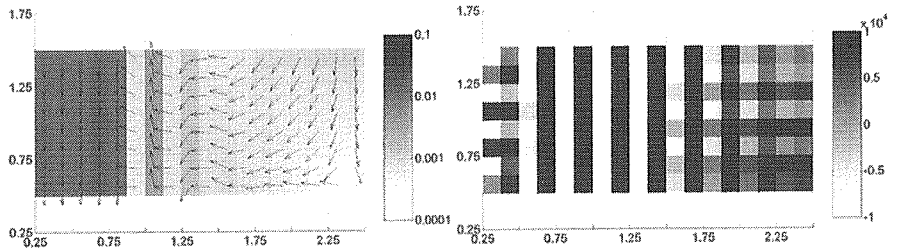

(a) Case 1: Fluid Velocities (b) Case 1: Fluid Pressure

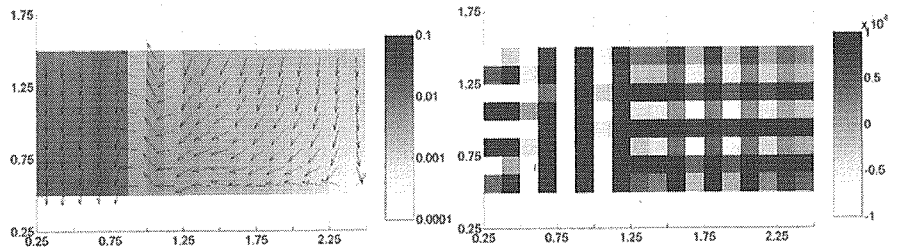

(c) Case 2: Fluid Velocities (d) Case 2: Fluid Pressure

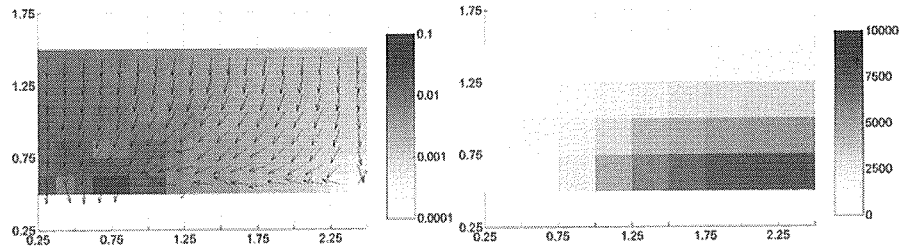

(e) Case 3: Fluid Velocities (f) Case 3: Fluid Pressure

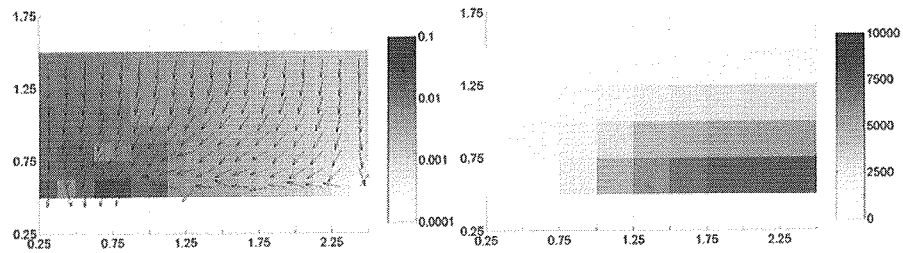

(g) Case 4: Fluid Velocities (h) Case 4: Fluid Pressure

Figure 2: Fluid velocities and pressure for cases 1-4.

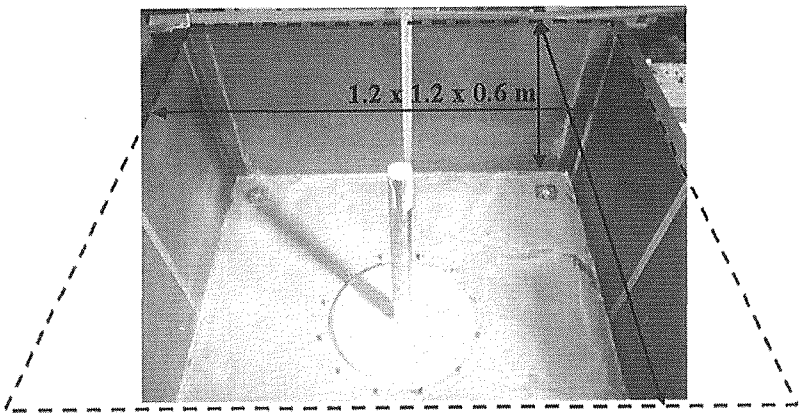

Figure 3: View inside the experiment box

It is interesting that in the saturated case soil far away from the fault is deformed. The horizontal solid lines added as guides to the eye to see the upward bending of the soil when approaching the fault. It seems that the negative pore water pressure (according to measurement performed during the experiment, but not shown here) increases the failure strength of the soil, which then behaves elastically for a larger deformation than in the case of the dry sand. Also the surface deformation shows a different character as seen in Figure 4

FAULT SURFACE RUPTURE SIMULATIONS

A hypo-plastic model (Herle and Gudehus, 1999) which is capable of modeling many of important characteristics of the soil is employed to describe the behavior of dense toyoura sand used in the experiment (see 4 for a simple description of input parameters and values. A detailed description is given in the reference above). Figure 5 shows the maximum shear strain after a total uplift of 10 cm in 40 cm deep and 60 cm wide soil deposit for a dry soil.

For the saturated case the results suffers from checker board effects of the pressure instability mentioned in the previous section as seen in Figure 6, which shows the maximum shear strains and fluid velocities at a 2 cm uplift of the base rock. The fluid velocities flow downwards and towards the dilating soil within the shear band.

An extension to circumvent the incompressibility related problems by using element strain increment averaging in combination with viscous or elastic hourglass control (Flanagan and Belytschko, 1981) is currently under investigation. Possibly a more recent extension of the hour-glass control could be implemented (Küssner and Reddy, 2001).

Table 3: Cases

Case	Normal Strain	B-bar	Averaging of fluid pressures
1	X		
2		X	
3	X		X
4		X	X

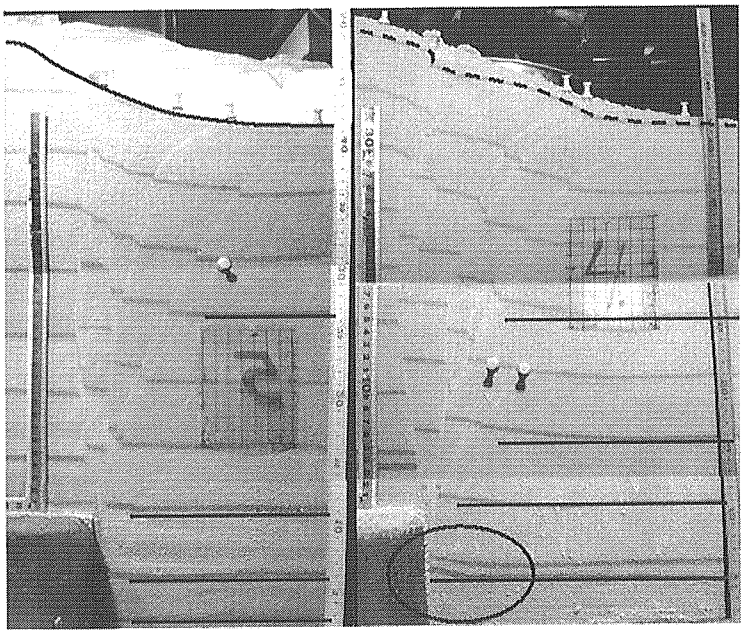

(a) Dry sand (b) Wet sand

Figure 4: Dry and Saturated Fault Experiment

CONCLUSIONS

Even though some numerical difficulties related to incompressibility remains to be solved the simple numerical scheme shows great promise for modeling large deformations of saturated soil deposits. Several different ways of computing strains were tried out for the seepage problem whereas for the saturated case only the b-bar method is presented here. Element strain increment averaging has also been tried out but hour-glassing deformations are quite large so some type of hour-glass control is necessary. Currently a way of circumventing the incompressibility problem for the solid part is under development and will be presented in a future publication.

Table 4: Hypo-plastic and fluid parameters.

Parameter	Value	Unit	Description
φ_c	30.0	[^{o}]	Critical state friction angle
h_s	2600.0e6	[Pa=N/m^2]	Stiffness parameter
n	0.27	[1]	Stiffness
e_{d0}	0.61	[1]	Minimum void ratio in stress free condition
e_{c0}	0.98	[1]	Critical state void ratio in stress free condition
e_{i0}	1.1	[1]	Maximum void ratio in stress free condition
α	0.18	[1]	fitting parameter
β	1.1	[1]	fitting parameter
$e_{initial0}$	0.65	[1]	Initial void ratio (measured in experiment)
E_{small}	100	Pa	Very small confining pressure stiffness (for numerical stability)
K_f	$1.0 \cdot 10^8$	Pa	Fluid bulk modulus

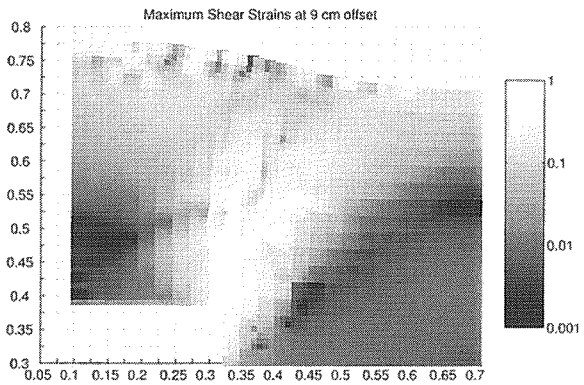

Figure 5: Maximum shear strains for dry case. Observe the logarithmic strain scale, 1=100% strain.

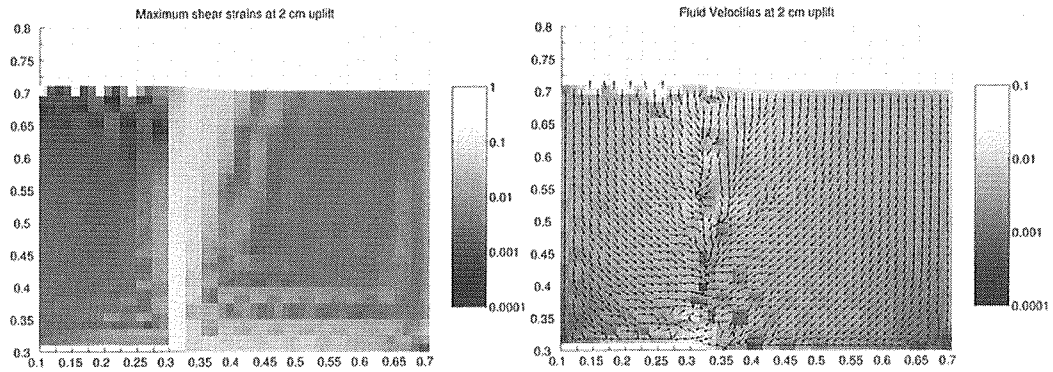

Figure 6: Maximum shear strains (a) and fluid velocities (b) for saturated case . Observe the logarithmic scales: (a) 1=100% strain, (b) [m/s]

APPENDIX EXPLICIT EXPRESSIONS FOR SOLID AND FLUID VELOCITIES

A somewhat lengthy derivation of explicit formulas for the solid and fluid velocities follows below.

The terms in the first parenthesis in Equation (43) can be further simplified to

$$\left(\tilde{M}_I+\frac{\Delta t}{2}\tilde{C}_I\right)^{-1}=\begin{bmatrix} M_{mI}+\frac{\Delta t}{2}C_{mI} & M_{cI} \\ M_{cI} & M_{fI}+\frac{\Delta t}{2}C_{fI}\end{bmatrix}^{-1}=$$

$$=\frac{1}{\left(M_{mI}+\frac{\Delta t}{2}C_{mI}\right)\left(M_{fI}+\frac{\Delta t}{2}C_{fI}\right)-M_{cI}^2}\begin{bmatrix} M_{fI}+\frac{\Delta t}{2}C_{fI} & -M_{cI} \\ -M_{cI} & M_{mI}+\frac{\Delta t}{2}C_{mI}\end{bmatrix} \tag{A1}$$

Calling the fraction in Equation (A1) Q, the explicit form of velocities which are suitable for direct implementation in a computer code becomes

$$\begin{aligned}\dot{u}_{Ii}^{k+1/2}=&Q\left(M_{fI}+\frac{\Delta t}{2}C_{fI}\right)\left[\Delta t\left(f_{mIi}^{ext,tractions}+f_{mIi}^{bodyforces}-f_{mIi}^{int}\right)+\right.\\&\left.\left(M_{mI}-\frac{\Delta t}{2}C_{mI}\right)\dot{u}_{Ii}^{k-1/2}+M_{cI}\dot{w}_{Ii}^{k-1/2}\right]-\\&QM_{cI}\left[\Delta t\left(f_{fIi}^{ext,pressure}+f_{fIi}^{bodyforces}+f_{fIi}^{int}\right)+\right.\\&\left.M_{cI}\dot{u}_{Ii}^{k+1/2}+\left(M_{fI}-\frac{\Delta t}{2}C_{fI}\right)\dot{w}_{Ii}^{k-1/2}\right]\end{aligned} \tag{A2}$$

and

$$\begin{aligned}\dot{w}_{Ii}^{k+1/2}=&-QM_{cI}\left[\Delta t\left(f_{mIi}^{ext,tractions}+f_{mIi}^{bodyforces}-f_{mIi}^{int}\right)+\right.\\&\left.\left(M_{mI}-\frac{\Delta t}{2}C_{mI}\right)\dot{u}_{Ii}^{k-1/2}+M_{cI}\dot{w}_{Ii}^{k-1/2}\right]+\\&Q\left(M_{mI}+\frac{\Delta t}{2}C_{mI}\right)\left[\Delta t\left(f_{fIi}^{ext,pressure}+f_{fIi}^{bodyforces}+f_{fIi}^{int}\right)+\right.\\&\left.M_{cI}\dot{u}_{Ii}^{k+1/2}+\left(M_{fI}-\frac{\Delta t}{2}C_{fI}\right)\dot{w}_{Ii}^{k-1/2}\right].\end{aligned} \tag{A3}$$

Collecting terms related to the mixture velocity, $\dot{u}_{Ii}$, and related to fluid velocity, $\dot{w}_{Ii}$, respectively, Equations (A2) and (A3) becomes

$$\begin{aligned}\dot{u}_{Ii}^{k+1/2} =& Q\left(\left(M_{fI}+\frac{\Delta t}{2}C_{fI}\right)\left(M_{mI}-\frac{\Delta t}{2}C_{mI}\right)-M_{cI}^2\right)\dot{u}_{Ii}^{k-1/2}+\\ & Q\Delta t\left(M_{fI}+\frac{\Delta t}{2}C_{fI}\right)\left(f_{mIi}^{ext,tractions}+f_{mIi}^{bodyforces}-f_{mIi}^{int}\right)+\\ & -QM_{cI}\Delta t\left(f_{fIi}^{ext,pressure}+f_{fIi}^{bodyforces}+f_{fIi}^{int}\right)+\\ & Q\left(\left(M_{fI}+\frac{\Delta t}{2}C_{fI}\right)M_{cI}-M_{cI}\left(M_{fI}-\frac{\Delta t}{2}C_{fI}\right)\right)\dot{w}_{Ii}^{k-1/2}\end{aligned} \tag{A4}$$

$$\begin{aligned}\dot{w}_{Ii}^{k+1/2} =& Q\left(-M_{cI}\left(M_{mI}-\frac{\Delta t}{2}C_{mI}\right)+\left(M_{mI}+\frac{\Delta t}{2}C_{mI}\right)M_{cI}\right)\dot{u}_{Ii}^{k-1/2}+\\ & -QM_{cI}\Delta t\left(f_{mIi}^{ext,tractions}+f_{mIi}^{bodyforces}-f_{mIi}^{int}\right)+\\ & Q\left(M_{mI}+\frac{\Delta t}{2}C_{mI}\right)\left(\Delta t\left(f_{fIi}^{ext,pressure}+f_{fIi}^{bodyforces}+f_{fIi}^{int}\right)\right)+\\ & Q\left(-M_{cI}M_{cI}+\left(M_{mI}+\frac{\Delta t}{2}C_{mI}\right)\left(M_{fI}-\frac{\Delta t}{2}C_{fI}\right)\right)\dot{w}_{Ii}^{k-1/2}\end{aligned} \tag{A5}$$

To update the velocities of the material points the nodal acceleration or velocity increments,

$$\Delta\dot{u}_{Ii}^{k}=\Delta t\ddot{u}_{Ii}^{k}=\left(\dot{u}_{Ii}^{k+1/2}-\dot{u}_{Ii}^{k-1/2}\right) \tag{A6}$$

and the fluid velocity increments

$$\Delta\dot{w}_{Ii}^{k}=\Delta t\ddot{w}_{Ii}^{k}=\left(\dot{w}_{Ii}^{k+1/2}-\dot{w}_{Ii}^{k-1/2}\right) \tag{A7}$$

are necessary. Putting Equations (A4) and (A5) into Equations (A6) and (A7), respectively give the increments

$$\begin{aligned}\Delta\dot{u}_{Ii}^{k} =& Q\left(\left(M_{fI}+\frac{\Delta t}{2}C_{fI}\right)\left(M_{mI}-\frac{\Delta t}{2}C_{mI}\right)-M_{cI}^2-\frac{1}{Q}\right)\dot{u}_{Ii}^{k-1/2}+\\ & Q\Delta t\left(M_{fI}+\frac{\Delta t}{2}C_{fI}\right)\left(f_{mIi}^{ext,tractions}+f_{mIi}^{bodyforces}-f_{mIi}^{int}\right)+\\ & -QM_{cI}\Delta t\left(f_{fIi}^{ext,pressure}+f_{fIi}^{bodyforces}+f_{fIi}^{int}\right)+\\ & Q\left(\left(M_{fI}+\frac{\Delta t}{2}C_{fI}\right)M_{cI}-M_{cI}\left(M_{fI}-\frac{\Delta t}{2}C_{fI}\right)\right)\dot{w}_{Ii}^{k-1/2}\end{aligned} \tag{A8}$$

and

$$\begin{aligned}\Delta\dot{w}_{Ii}^{k} =& Q\left(-M_{cI}\left(M_{mI}-\frac{\Delta t}{2}C_{mI}\right)+\left(M_{mI}+\frac{\Delta t}{2}C_{mI}\right)M_{cI}\right)\dot{u}_{Ii}^{k-1/2}+\\ & -QM_{cI}\Delta t\left(f_{mIi}^{ext,tractions}+f_{mIi}^{bodyforces}-f_{mIi}^{int}\right)+\\ & Q\left(M_{mI}+\frac{\Delta t}{2}C_{mI}\right)\left(\Delta t\left(f_{fIi}^{ext,pressure}+f_{fIi}^{bodyforces}+f_{fIi}^{int}\right)\right)+\\ & Q\left(-M_{cI}^2+\left(M_{mI}+\frac{\Delta t}{2}C_{mI}\right)\left(M_{fI}-\frac{\Delta t}{2}C_{fI}\right)-\frac{1}{Q}\right)\dot{w}_{Ii}^{k-1/2}\end{aligned} \tag{A9}$$

Expanding Q inside the parenthesizes gives

$$\begin{aligned}\Delta\dot{u}_{Ii}^{k} =& Q\left[\left(M_{fI}+\frac{\Delta t}{2}C_{fI}\right)\left(M_{mI}-\frac{\Delta t}{2}C_{mI}\right)-M_{cI}^{2}+\right.\\ &\left.-\left(\left(M_{mI}+\frac{\Delta t}{2}C_{mI}\right)\left(M_{fI}+\frac{\Delta t}{2}C_{fI}\right)-M_{cI}^{2}\right)\right]\dot{u}_{Ii}^{k-1/2}+\\ & Q\Delta t\left(M_{fI}+\frac{\Delta t}{2}C_{fI}\right)\left(f_{mIi}^{ext,tractions}+f_{mIi}^{bodyforces}-f_{mIi}^{int}\right)+\\ & -QM_{cI}\Delta t\left(f_{fIi}^{ext,pressure}+f_{fIi}^{bodyforces}+f_{fIi}^{int}\right)+\\ & Q\left(\left(M_{fI}+\frac{\Delta t}{2}C_{fI}\right)M_{cI}-M_{cI}\left(M_{fI}-\frac{\Delta t}{2}C_{fI}\right)\right)\dot{w}_{Ii}^{k-1/2}\end{aligned} \tag{A10}$$

and

$$\begin{aligned}\Delta\dot{w}_{Ii}^{k} =& Q\left(-M_{cI}\left(M_{mI}-\frac{\Delta t}{2}C_{mI}\right)+\left(M_{mI}+\frac{\Delta t}{2}C_{mI}\right)M_{cI}\right)\dot{u}_{Ii}^{k-1/2}+\\ & -QM_{cI}\Delta t\left(f_{mIi}^{ext,tractions}+f_{mIi}^{bodyforces}-f_{mIi}^{int}\right)+\\ & Q\left(M_{mI}+\frac{\Delta t}{2}C_{mI}\right)\left(\Delta t\left(f_{fIi}^{ext,pressure}+f_{fIi}^{bodyforces}+f_{fIi}^{int}\right)\right)+\\ & Q\left[-M_{cI}^{2}+\left(M_{mI}+\frac{\Delta t}{2}C_{mI}\right)\left(M_{fI}-\frac{\Delta t}{2}C_{fI}\right)+\right.\\ & \left.-\left(\left(M_{mI}+\frac{\Delta t}{2}C_{mI}\right)\left(M_{fI}+\frac{\Delta t}{2}C_{fI}\right)-M_{cI}^{2}\right)\right]\dot{w}_{Ii}^{k-1/2}\end{aligned} \tag{A11}$$

Canceling terms of opposite signs the following two equations are obtained:

$$\begin{aligned}\Delta\dot{u}_{Ii}^{k} =& Q\left(M_{fI}+\frac{\Delta t}{2}C_{fI}\right)(-\Delta tC_{mI})\dot{u}_{Ii}^{k-1/2}+\\ & Q\Delta t\left(M_{fI}+\frac{\Delta t}{2}C_{fI}\right)\left(f_{mIi}^{ext,tractions}+f_{mIi}^{bodyforces}-f_{mIi}^{int}\right)+\\ & -QM_{cI}\Delta t\left(f_{fIi}^{ext,pressure}+f_{fIi}^{bodyforces}+f_{fIi}^{int}\right)+\\ & Q\Delta tM_{cI}C_{fI}\dot{w}_{Ii}^{k-1/2}\end{aligned} \tag{A12}$$

$$\begin{aligned}\Delta\dot{w}_{Ii}^{k} =& QM_{cI}\Delta tC_{mI}\dot{u}_{Ii}^{k-1/2}+\\ & -QM_{cI}\Delta t\left(f_{mIi}^{ext,tractions}+f_{mIi}^{bodyforces}-f_{mIi}^{int}\right)+\\ & Q\left(M_{mI}+\frac{\Delta t}{2}C_{mI}\right)\left(\Delta t\left(f_{fIi}^{ext,pressure}+f_{fIi}^{bodyforces}+f_{fIi}^{int}\right)\right)+\\ & Q\left(M_{mI}+\frac{\Delta t}{2}C_{mI}\right)(-\Delta tC_{fI})\dot{w}_{Ii}^{k-1/2}\end{aligned} \tag{A13}$$

Collecting terms we finally get

$$\Delta \dot{u}_{Ii}^{k} = Q\Delta t \left[-\left(M_{fI} + \frac{\Delta t}{2} C_{fI} \right) C_{mI} \dot{u}_{Ii}^{k-1/2} + M_{cI} C_{fI} \dot{w}_{Ii}^{k-1/2} + \left(M_{fI} + \frac{\Delta t}{2} C_{fI} \right) \left(f_{mIi}^{ext,tractions} + f_{mIi}^{bodyforces} - f_{mIi}^{int} \right) + - M_{cI} \left(f_{fIi}^{ext,pressure} + f_{fIi}^{bodyforces} + f_{fIi}^{int} \right) \right] \tag{A14}$$

$$\Delta \dot{w}_{Ii}^{k} = Q\Delta t \left[M_{cI} C_{mI} \dot{u}_{Ii}^{k-1/2} - \left(M_{mI} + \frac{\Delta t}{2} C_{mI} \right) C_{fI} \dot{w}_{Ii}^{k-1/2} + - M_{cI} \left(f_{mIi}^{ext,tractions} + f_{mIi}^{bodyforces} - f_{mIi}^{int} \right) + \left(M_{mI} + \frac{\Delta t}{2} C_{mI} \right) \left(f_{fIi}^{ext,pressure} + f_{fIi}^{bodyforces} + f_{fIi}^{int} \right) \right]. \tag{A15}$$

REFERENCES

Bardenhagen, S. G. (2002). Energy conservation error in the material point method for solid mechanics. *Journal of Computational Physics*, 180:383–403.

Bathe, K. (1996). *Finite element procedures*. Prentice-Hall.

Burgess, D., Sulsky, D., and Brackbill, J. (1992). Mass matrix formulation of the flip particle in cell method. *J. Comp. Phys.*, 103:1–15.

Chan, A., Famiyesin, O., and Wood, M. D. (1991). A fully explicit u-w scheme for dynamic soil and pore fluid interaction. In Cheung, Lee, and Leung, editors, *Asian Pacific Conference on Computational Mechanics*, pages 881–887. Balkema, Rotterdam.

Flanagan, D. P. and Belytschko, T. (1981). A uniform strain hexahedron and quadrilateral with orthogonal hourglass control. *International Journal of Numerical Methods in Engineering*, 17:679–706.

Harlow, F. H. (1964). The particle-in-cell computing method for fluid dynamics in fundamental methods in hydrodynamics. In *Experimental Arithmetic, High-Speed Computations and Mathematics*, pages 319–345. Academic Press.

Herle, I. and Gudehus, G. (1999). Determination of parameters of a hypoplastic constitutive model from properties of grain assemblies. *Mech. Cohes.-Frict. Mater.*, 4:461–486.

Hughes, T. J. R. (1983). Numerical implementation of consitutive models: Rate-independant deviatoric plasticity. In *Theoretical foundation for large-scale computations of nonlinear material behavior*, pages 29–64. Martinus Nijhoff Publishers.

Kolymbas, D. (19??). *An introduction to hypoplasticity*. ??

Küssner, M. and Reddy, B. D. (2001). The equivalent parallelogram and parallelipiped, and their application to stabilised finite elements in two and three dimensions. *Computer Methods in Applied Mechanics and Engineering*, 190:1967–1983.

Lewis, R. and Schrefler, B. (1998). *The finite element method in the static and dynamic deformation and consolidation porous media*. John Wiley and Sons, West Sussex, England, 2 edition.

Mukoyama, S. (2000). Fault induced surface configuration features (in japanese). In *Mountain Geomorphology*, pages 82–100. Kokonshoin Press.

Nagtegaal, J., Rice, D. M., and Park, J. R. (1974). On numerically accurate finite element solutions in the fully plastic range. *Comput. Methods Appl. Mech. Engrg.*, 4:153–177.

Sulsky, D., Chen, Z., and Schreyer, H. L. (1994). A particle method for history-dependent materials. *Comput. Methods Appl. Mech. Engrg.*, 118:179–196.

Sulsky, D., Zhou, S. J., and Schreyer, H. L. (1995). Application of particle-in-cell method to solid mechanics. *Comp. Phys. Comm.*, 87:236–252.

Wieckowski, Z., Youn, S.-K., and Yeon, J.-H. (1999). A particle-in-cell solution to the silo discharging problem. *International Journal of Numerical Methods in Engineering*, 45:1203–1225.

Zienkiewicz, O., Chan, A., Pastor, M., Paul, D., and Shiomi, T. (1990). Static and dynamic behaviour of geomaterials - a rational approach to quantitative solutions, part i: Fully saturated problems. *Proc. Roy. Soc. London*, A429:285–309.

Zienkiewicz, O., Chan, A., Pastor, M., Schrefler, B., and Shiomi, T. (1999). *Computational geomechanics with special reference to earthquake engineering*. John Wiley and Sons, West Sussex, England.